ISBN: 978-3-95450-194-6 doi:10.18429/JACoW-LINAC2018-MOPO008

THE RF GUN ADOPTING THE DIELECTRIC ASSIST ACCELERATING STRUCTURE

Shingo Mori*, Mitsuhiro Yoshida†, KEK, Tsukuba, Japan
Daisuke Satoh‡, National Institute of Advanced Industrial Science and Technology, Tsukuba, Japan

Abstract

We apply the dielectric assist accelerating (DAA) structure to the RF gun, which is a candidate for a high average current and high brightness electron source. The DAA structure consists of ultralow-loss dielectric cylinders and disks which are periodically arranged in a metallic enclosure. Due to the high quality factor and the high shunt impedance of the DAA cavity, the RF gun adopting the DAA cavity can be a high-duty electron beam source at room temperature. We provide design work for RF gun adopting the DAA structure.

INTRODUCTION

The RF photoinjectors have been widely used as a source of high-quality beam. The electron beam of low emittance and high beam current are now considered as the electron sources for the x-ray free electron laser (FEL) which requires lower emittance to obtain shorter wavelengths and high peak current to obtain good gain, and linear colliders to meet the requirement of a complex pulse structure and to provide small emittance flat beam [1].

The first use of the RF photoinjector was done by Fraser et al. [2] in 1985 at LANL for the application to the FEL. The idea to combine a photocathode and a laser system with an RF cavity that supports a standing-wave field has many advantages. First, the electron bunch length is determined by the laser pulse without the following buncher section and provides narrow energy spread. Second, the electron beam is immediately accelerated up to relativistic energy by high RF field on the cathode within the first cell, which can decrease the space-charge growth of the emittance when the electrons are non-relativistic. Third, the quite low emittance beams can be produced by decreasing the laser spot size at the photocathode [3] which can reach as small emittance as 0.1 mm · mrad with relatively small bunch charge $>$ 0.1 nC. The electron beam dynamics after generation from the cathode is well understood analytically [4, 5] and numerically. The emittance of the beam produced by the RF electron gun is determined by three contributions: the emittance as the bunch emerges from the cathode; the electromagnetic interaction among the non-relativistic electrons called as the space charge effect; nonlinear radial dependence of the transverse components of RF.

In most cases, the RF photoinjector operates at a low duty factor and have relatively low average current. The first photoinjector with a duty factor of 25% was designed by Boeing in 1992 [6]. Currently, a collaboration between LANL and AES is developing a normal conducting photoinjector, which works in the CW mode. In the CW mode operation of a normal conducting photoinjector, the large amount of RF power loss causes cooling problems and bounds the gradient, e.g. 7 MV/m in ref. [6], which becomes drawbacks in the emittance. While superconducting RF photoinjectors also provides CW mode operation with high average current, with low emittance $O(1)$ mm · mrad due to the moderate gradient 20-50 MV/m.

A dielectric assist accelerating (DAA) structure [7, 8] is promising in power efficiency and could be a new candidate of photoinjector with CW mode operation, because it provides high efficiency $Q \sim O(10^5)$ at room temperature. Due to the structures of the dielectrics and the use of the ultra-low-loss dielectric material [8], the five cell DAA cavity provides the Q-value, $Q = O(10^5)$, and the shunt impedance $Z_{sh} \simeq 650$ MΩ/m. We have constructed the test stand for the DAA test cavity whose design frequency is 5712 MHz. In the tentative high voltage test, we found the gradient can reach up to multi-MV/m. This test cavity is planned to examine the main cavity to accelerate a relativistic electron beam which is generated from the RF photoinjector. In order to examine the possibility of the high-duty operation of the DAA main cavity, it is reasonable to construct the RF photoinjector which applies the DAA structure as well.

In order to investigate the possibility of the DAA structure as an RF photoinjector, we carry out the numerical calculation of the electromagnetic field in the cavity and the coupler, and the dynamics of an electron bunch generated by the photocathode.

This paper is organized as follows. In Sec.2, the dielectric cell of the DAA structure is introduced and we discuss the boundary problem which appear when the beam hole opens. In Sec.3, we introduce the novel structure of the end cell to avoid the boundary problem. In Sec.4, we will show the numerical result of the RF photoinjector based on the DAA structure. In Sec.5, we will summarize our result.

THE DAA STRUCTURE AND THE BOUNDARY PROBLEM

In this section, we will review the concept of the DAA structure and its boundary effect.

The basic structure of the DAA cavity is periodic, which is composed of the cylindrical waveguide made of metal and a cell called regular cell. Figure 1 shows the distribution of the electric force line calculated using *SUPERFISH* in the pillbox cavity which contains a regular cell. We call the

* smori@post.kek.jp
† mitsuhiro.yoshida@kek.jp
‡ dai-satou@aist.go.jp

ISBN: 978-3-95450-194-6 doi:10.18429/JACoW-LINAC2018-MOPO008

horizontal axis and vertical axis as z and r direction, which describe the beam axis and radial direction of the dielectric cell. The dielectric cell is the combination of the disk-like structure and the coaxial structure, which are shown as the rectangular region around $z \in (1, 1.5)$ cm and the horizontal region around $r \sim 2.5$ cm, respectively. *SUPERFISH* provides us the electromagnetic field distribution in the frequency domain in (z, r) coordinates assuming the rotational symmetry about the beam axis. The red lines denote the real part of the electric force line and the green lines shows the imaginary part of them, which describe the magnitude of the accelerating field $E_z(z, r)$ has maximum value at the beam axis.

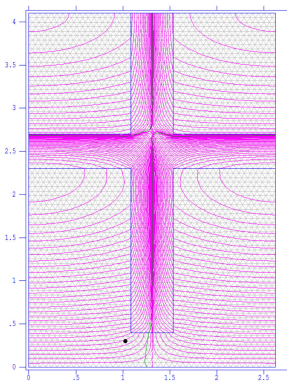

Figure 1: The electric field configuration in the frequency domain calculated by *SUPERFISH*. The ticks denote the dimension in cm unit. This figure describes the field configuration of the design frequency of the test cavity, i.e. 5712 MHz. The red curves denotes the electric force line.

In Fig. 1, the electric field is the standing wave along the z-direction and has periodic structure due to the metal walls on the left and the right side. The whole field configuration inside the DAA cavity is similar to the TM_{02n} mode in the pillbox cavity, whose difference appears from the dielectric cells. The dimensions of the dielectric structure are determined so that the peaks of the electric field is confined within the ceramics which has relatively high permittivity, $\epsilon_r \sim 10$ and can hold many electric force lines.

The structure of the DAA cavity has advantage of the high Q-value and the high shunt impedance as described below. As for the Q-value, the coaxial dielectric layer partially confines the electromagnetic field in the cavity so that the surface magnetic field at the copper surface becomes relatively small compared to one of the pillbox cavity. As for the shunt impedance, it is known that the waveguides with dielectric disks have a higher shunt impedance than all-metal waveguides [9]. Naively, this is because the dielectric disks make the electric force line concentrated around the beam axis, which is also applied in the DAA structure.

Due to the efficient structure to keep the RF energy and concentrate them to the beam axis, the result of the simulation shown in Fig. 1 is $Q = 1.4 \times 10^5$ and $Z_{\rm sh} \simeq 900\ {\rm M}\Omega/{\rm m}$. However, once the beam hole opens, the figures of merit significantly decrease by around 80%.

In the large number of cells limits, the effect of the beam hole to the cavity parameters is negligible. If the cavity contains $N_{\rm cell}$ regular cells, the boundary cells of the both ends effect by $2/N_{\rm cell}$ in the figure of merit of the whole cavity. However, in the test DAA cavity shown in Fig. 2, we apply $N_{\rm cell} = 6$ and boundary effect is huge. In order to avoid the reduction from the boundary effect, we apply additional cylinder in the end cell, which is shown in $r \in [0.5, 1]$ and $z \in [0.5, 2]$ in Fig. 2, so that most of the electric force lines hit above the beam hole and electric field around beam hole becomes smaller. Applying the end-cell structure, we obtained $Q = 1.2 \times 10^5$ and $Z_{\rm sh} \sim 600\ {\rm M}\Omega/{\rm m}$.

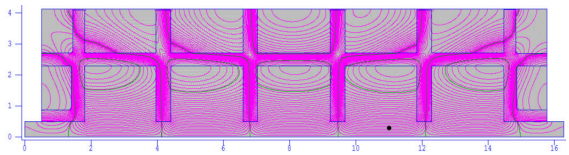

Figure 2: The electric field configuration in the frequency domain calculated by *SUPERFISH*. The ticks denotes the dimension in cm unit. This figure describes the field configuration of the design frequency of the test cavity, i.e. 5712 MHz. The red curves denotes the electric force line.

The above naive solution still causes a new problem that the symmetry of the field in terms of each disk is broken by the boundary effect. Moreover, the peaks of the field across the surface of the dielectric cells which would cause the discharge in the high voltage test.

THE NOVEL END CELL STRUCTURE OF THE DAA CAVITY

We found a configuration shown in Fig. 3 which can confine the field in the dielectric cells approximately restoring the symmetry even the neighboring cell of the end cell, which can also optimize the figures of merit.

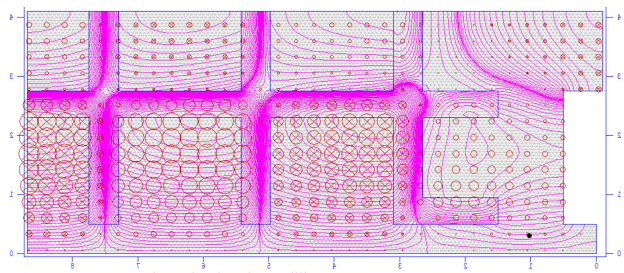

Figure 3: The electric field configuration in the frequency domain calculated by *SUPERFISH*. The ticks denotes the dimension in cm unit. This figure describes the field configuration of the design frequency of the optimized end cell, i.e. 5712 MHz. The red curves denotes the electric force line.

The class of field configurations like Fig. 3 can be reproduced by considering the interference condition along z di-

ISBN: 978-3-95450-194-6 doi:10.18429/JACoW-LINAC2018-MOPO008

rection. In Fig. 4, we show a schematic figure to explain the concept of the end cell structure. The gray region denotes the dielectrics and the white region denotes the vacuum. The parameters a, b, c, δ, d, and D are numerically determined so that the field configuration in the regular cell is optimized in terms of the Q-value and the shunt impedance. Other three parameters, l_1, l_2, and l_3 are determined as below. Compared with the regular cell shown in Fig. 1, here we introduce an additional dielectric cylinder near the beam hole with a length of l_1 and a vacuum region with a length of l_2. Considering the optical path length of the path1 and the path2 which are shown in Fig. 4 as L_1 and L_2, since the refractive index n of the dielectric cell is greater than one, apparently they should satisfy $L_1 < L_2$. As the length of a regular cell corresponds to a half wavelength, it is natural to consider the interference conditions, $L_1 = \lambda$, $L_2 = 3\lambda/2$, which determine two parameters, l_1 and l_2. We found the field configuration calculated with the dimensions l_1 and l_2 obtained as above can improve both Q and Z_{sh}. Then, we tune the third parameter l_3 in order to confine the electric force lines in the dielectrics and optimize the Q-value and the shunt impedance, further.

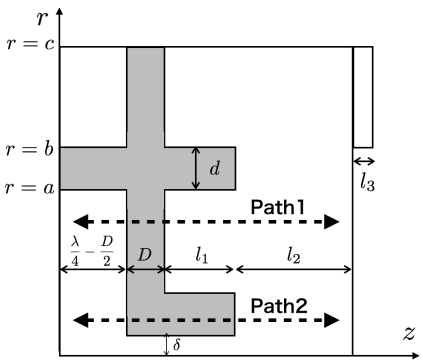

Figure 4: The schematic picture of the new end cell structure.

THE APPLICATION OF THE DAA CELL TO THE RF PHOTO INJECTOR

In this section, we show the numerical result of the particle-in-cell simulation using *CST MICROWAVE STUDIO* (CST) in the RF photoinjector applying the DAA structure. In the following calculation, we adopt the end cell shown in Fig. 3. Since the high power test of the DAA cavity has not been completed and tens of MV/m region has not been established yet, we assume the moderate value for the accelerating gradient, i.e. 20 MV/m. Although the DAA test cavity is designed to work with the frequency of 5712 MHz, the RF frequency of 5712 MHz is too high, in the gradient assumed here, to accelerate non-relativistic electrons bunches generated at the cathode up to relativistic energy within the first half cell. Thus, we adopt a frequency of 2856 MHz as the design frequency, which enlarges all the dimensions of the cavity in Fig. 3 by a factor of two.

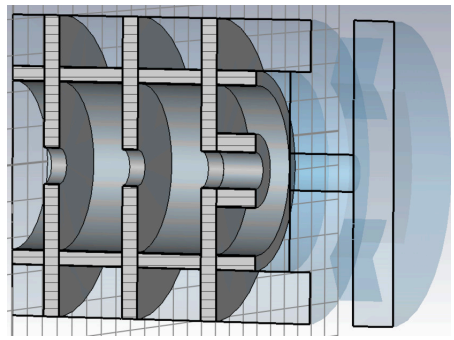

Figure 5: The RF photoinjector and the coupler used in our simulation.

Figure 5 shows the picture of the DAA applied RF photoinjector. We introduce a coupler between the waveguide and the cavity as four coaxial holes which are on the periphery of the cavity, so that the iris of the beam hole can be minimized keeping the coupling large. Due to the parity symmetry of the system in terms of the x-z plane and the y-z plane, we apply the symmetry condition to reduce the calculation cost as $H_t = 0$ on the both planes.

In Fig. 6, we show the distribution of the electric field in unit of V/m in the (z, r) plane calculated by CST. In Fig. 7, we show the magnetic field in unit of A/m in the (z, r) plane calculated by CST.

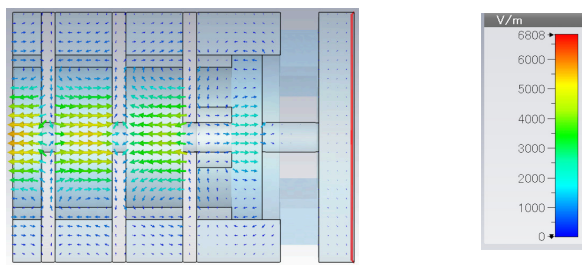

Figure 6: The contour plot of the tangential component of the electric field calculated using CST.

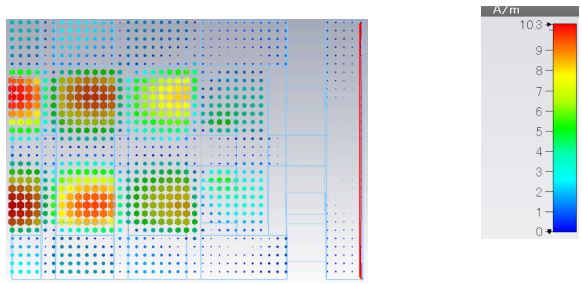

Figure 7: The contour plot of the normal component of the magnetic field calculated using CST.

In Fig. 8, we show the distribution of the gradient on the beam axis normalized by the maximum magnitude of it, $E_z(z, r = 0)/E_z(z = 0, r = 0)$, and the phase, $\mathrm{Arg}(E_z(z, r =$

ISBN: 978-3-95450-194-6 doi:10.18429/JACoW-LINAC2018-MOPO008

0)), calculated by CST as blue dots and orange dots, respectively. The plot shows the field configuration when the amplitude of the electric field is maximum. As expected from the coupler structure, the gradient outside the cavity is suppressed well.

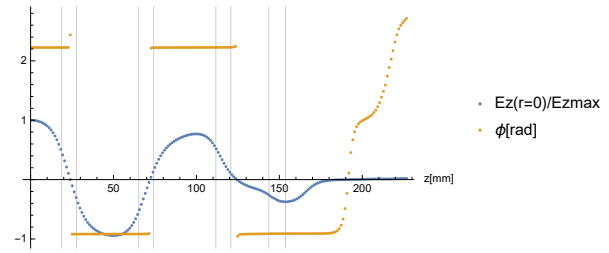

Figure 8: The accelerating field $E_z(z, r = 0)$ calculated by numerical simulation.

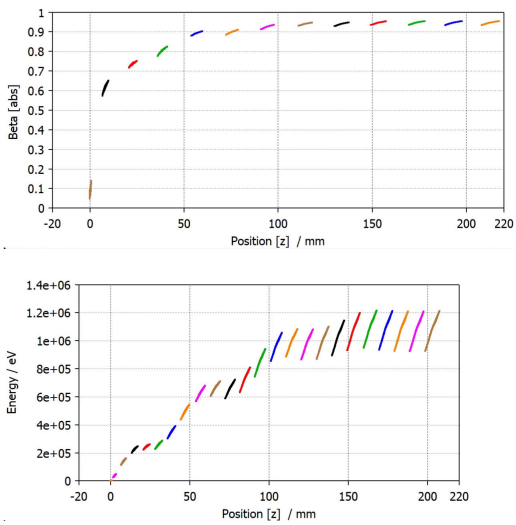

Figure 9: The z dependence, namely time dependence, of the β distribution and the energy distribution of a bunch calculated by CST.

The upper and lower figures in Fig. 9 show the β-z distribution and the Energy-z distribution in a bunch for each time step with a step size of 52 ps, respectively. Apparently, the electrons become relativistic at the exit of the RF cavity.

In Table 1, we show the parameters used in our calculation and beam parameters measured at the outside of the cavity. In our analysis, we synchronize the laser pulse and the RF phase so that emitted electron bunches are maximally accelerated in the first half cell. We numerically estimate the thermal loss in the cavity to support the gradient of 20 MV/m, which is about 290 kW in our simulation. At present, the water cooling can remove the power deposited as the surface temperature, whose typical capacity is 100 kW, which corresponds to the duty factor about 34 %. In contrast, if we want to operate the system with the duty factor of 1 %, the cooling power required is about 2.9 kW.

Table 1: The Parameters Related to the RF and the Emittance

RF frequency [MHz]	2856
field on cathode [MV/m]	20
RF phase at cathode for laser pulse	$3\pi/2$
thermal loss [kW]	290
laser spot [σ in mm]	2.0
laser pulse width [σ in ps]	10
charge in bunch [nC]	0.1
ϵ_z at exit [mm · mrad]	1.5
ϵ_T at exit [mm · mrad]	1.3
beam energy spread at exit [%]	4.0
bunch length at exit [σ in mm]	1.5
bunch radius at exit [σ in mm]	1.5

The thermal loss contains two contributions from the surface of the cavity and the dielectric loss, whose power dissipation is 245 kW and 45 kW, respectively. The thermal conductivity of the ceramics we adopt is about ten times smaller than one of the pure copper, while the heating power generated at the dielectrics is around ten times smaller than one of the pure copper. Then, the difference of the thermal conductivity is canceled by the difference of the power loss.

CONCLUSION

The DAA structure is a candidate for the highly efficient accelerator which could realize the continuous-wave-mode operation at room temperature with a relatively larger current. We investigate the application of the DAA structure to the RF electron gun, which could provide the high-quality beam with high peak current.

In our analysis, the structure of the end cell appears to be important since the RF photoinjector is constructed from a small number of cells. First, we try to optimize the effect of opening the beam hole by introducing the vacuum region between the end cell and the wall, which weakens the strength of the field at the beam hole satisfying the interference conditions along z direction.

We apply the optimized structure to the DAA applied RF photoinjector and numerically investigate the behavior of a electron bunch generated at the cathode, which shows that a bunch with the normalized emittance of $O(1)$mm · mrad can be generated by the DAA adopted photoinjector. The duty factor of 1 % is possible with the cooling power of 2.9 kW. Considering the water cooling capacity of 100 kW the possible duty factor is 34 %.

ACKNOWLEDGEMENTS

This work is supported by JSPS KAKENHI Grant No. 16H02134. The authors would like to thank N. Shigeoka from the Mitsubishi Heavy Industries Mechatronics Systems Ltd. for their continued support of the development of DAA structures.

ISBN: 978-3-95450-194-6 doi:10.18429/JACoW-LINAC2018-MOPO008

REFERENCES

[1] R Brinkmann, Ya Derbenev, and K Flöttmann. A low emittance, flat-beam electron source for linear colliders. *Physical Review Special Topics-Accelerators and Beams*, 4(5):053501, 2001.

[2] JS Fraser, RL Sheffield, ER Gray, PM Giles, RW Springer, and VA Loebs. Photocathodes in accelerator application, ieee particle accelerator conf., washington, dc. In *IEEE Cat*, number 87CH2387-9, pages 1705–1709, 1987.

[3] Y Kim, A Andersson, M Dach, R Ganter, T Garvey, C Gough, CH Hauri, R Ischebeck, F Le Pimpec, M Paraliev, et al. Low thermal emittance measurements at the psi-xfel low emittance gun test facility. In *Proceeding of FEL*, volume 8, 2008.

[4] Kwang-Je Kim. Rf and space-charge effects in laser-driven rf electron guns. *Nuclear Instruments and Methods in Physics Research Section A: Accelerators, Spectrometers, Detectors and Associated Equipment*, 275(2):201–218, 1989.

[5] Bruce E Carlsten. New photoelectric injector design for the los alamos national laboratory xuv fel accelerator. *Nuclear Instruments and Methods in Physics Research Section A: Accelerators, Spectrometers, Detectors and Associated Equipment*, 285(1-2):313–319, 1989.

[6] DH Dowell, KJ Davis, KD Friddell, EL Tyson, CA Lancaster, L Milliman, RE Rodenburg, T Aas, M Bemes, SZ Bethel, et al. First operation of a photocathode radio frequency gun injector at high duty factor. *Applied physics letters*, 63(15):2035–2037, 1993.

[7] D Satoh, M Yoshida, and N Hayashizaki. Dielectric assist accelerating structure. *Physical Review Accelerators and Beams*, 19(1):011302, 2016.

[8] D Satoh, M Yoshida, and N Hayashizaki. Fabrication and cold test of dielectric assist accelerating structure. *Physical Review Accelerators and Beams*, 20(9):091302, 2017.

[9] LB Mullett, W Walkinshaw, JS Bell, BG Loach, et al. A theoretical and experimental investigation of anisotropic-dielectric-loaded linear electron accelerators. *Proceedings of the IEE-Part B: Radio and Electronic Engineering*, 104(15):273–290, 1957.